Advances in Science and Technology Research Journal

Advances in Science and Technology Research Journal, 2026, 20(7), 197–209
https://doi.org/10.12913/22998624/219122
ISSN 2299-8624, License CC-BY 4.0

Received: 2026.01.21
Accepted: 2026.05.15
Published: 2026.06.01

Aerodynamic research in the wind tunnel on a gyroplane model

Piotr Fiedoruk[1], Tomasz Łusiak[2], Jacek Dudziak[3*]

[1] General Command of the Armed Forces, ul. Żwirki i Wigury 103/105, 00-912 Warsaw, Poland
[2] Department of Thermodynamics, Fluid Mechanics and Aviation Propulsion Systems, Lublin University of Technology, ul. Nadbystrzycka 36, 20-618 Lublin, Poland
[3] Lukasiewicz Research Network – Institute of Aviation, Aviation Technologies Center, al. Krakowska 110/114, 02-256 Warsaw, Poland
* Corresponding author's e-mail: jacek.dudziak@ilot.lukasiewicz.gov.pl

ABSTRACT

This paper presents the results of an experimental investigation of a gyroplane model conducted in a low-speed wind tunnel. The primary objective of the study was to evaluate the aerodynamic characteristics of the complete configuration and selected partial configurations, including the cases without horizontal and vertical stabilisers. Measurements were performed for a range of fuselage angles of attack and sideslip angles to determine the influence of landing gear deployment, nacelle geometry, and tail surfaces on aerodynamic performance. The analysis included the assessment of lift, drag, and side force coefficients, as well as stability and control derivatives. The results indicated that the horizontal stabiliser provides sufficient longitudinal stability, as confirmed by the calculated Tail Volume Coefficient, while the nacelle form drag contributes significantly to the overall fuselage drag. Recommendations for future design improvements include optimization of nacelle shape and landing gear fairings to minimise drag and enhance lift during critical flight phases.

Keywords: wind tunnel, aerodynamic testing, gyroplane model, lift and drag, scale model testing.

INTRODUCTION

An autogyro is an aerial vehicle with a unique aerodynamic configuration in which the main lifting force is generated by a rotor operating in autorotation, while propulsion is provided by a separate propeller-driven power unit. This design results in aerodynamic characteristics that differ significantly from both fixed-wing aircraft and helicopters. Due to the specific behaviour of the rotor in autorotation, autogyros require dedicated aerodynamic investigations, including: analysis of the interaction between individual structural components and the resulting forces and moments, modelling of the airflow around the rotor under autorotative conditions, studies of the influence of the tailplane on longitudinal and lateral stability, and evaluation of various tail configurations [1].

The behaviour of an aircraft after the occurrence of disturbances, such as sudden variations in airflow velocity, is described by the properties of its undisturbed motion, commonly referred to as stability and steadiness. A necessary condition for maintaining steady flight is not only the equilibrium of all aerodynamic forces acting on the aircraft, but also the balance of moments around the three coordinate axes passing through its centre of gravity [2]. This equilibrium should be stable, meaning that after a disturbance – such as a gust of wind – the aircraft should return to its steady-state condition within a relatively short time, without pilot's intervention, provided that the disturbance remains within acceptable limits. For this reason, the concepts of equilibrium and stability are closely related [3]. Static stability describes the ability of an aircraft to return to its equilibrium position once the disturbing factor disappears, whereas dynamic stability characterises the nature of this return, including the number and amplitude of possible oscillations. These two

aspects are inseparably linked – an aircraft can only be dynamically stable if it is statically stable. Stability about the lateral axis (y-axis) is referred to as longitudinal stability and is ensured by the horizontal tail. Stability about the longitudinal (x) and vertical (z) axes, resulting from the action of the wings and vertical tail, is known as lateral and directional stability, respectively. In the literature, these are often considered together as lateral stability due to their strong interdependence [4].

The aerodynamic characteristics of airfoil profiles are determined in wind tunnels using procedures that allow the analysis of a profile of infinite span, which can then be translated to wings of any finite span. In the present case, only skin friction and profile drag are considered, while induced drag – typical for wings of finite span – is omitted. The minimum drag coefficient occurs at the angle of attack α_0 corresponding to zero lift, and its value increases along with airfoil thickness [5].

Aerodynamic characteristics provide essential information about the behaviour of airfoil profiles and enable the calculation of aircraft performance. The range of the aerodynamic polar typically includes angles of attack slightly exceeding the critical angle α_{kr}. The shape of the polar may vary depending on flight conditions, such as take-off, landing, climb, or maximum-speed flight, which results from changes in Reynolds number and the different configurations of aircraft components. The lift generated by the horizontal tail, which ensures the balance of longitudinal moments acting on the aircraft is also an important factor. Its magnitude varies with angle of attack, flight speed, and elevator deflection [6, 7].

Maximum aerodynamic efficiency K occurs at the angle of attack corresponding to the highest value of this parameter and determines, among other things, the maximum range of the aircraft. It is one of the key quantities describing the aerodynamic properties of an airfoil [8, 9].

In the available scientific literature, there is a noticeable lack of comprehensive and systematic studies on the aerodynamic characteristics of autogyros conducted in wind tunnels. Although a few publications examined selected configurations of aircraft, their number is limited and their scope remains narrow. For this reason, it is essential to bridge this research gap by performing dedicated wind-tunnel experiments, analysing the obtained results, and formulating conclusions that relate both to the aerodynamics of the investigated configurations and to the manufacturing quality of additively produced 3D models. Such an approach will not only enhance the understanding of aerodynamic phenomena specific to autogyros but also enable the development of concrete recommendations for the design, preparation, and validation of the 3D-printed models used in future studies.

Theoretical basis

Aerodynamics constitutes a foundational discipline in the engineering and operational performance of aircraft, exerting a profound influence on stability, manoeuvrability, and energy efficiency. Control surfaces – including the elevator, rudder, and ailerons – are integral to modulating aerodynamic moments and enabling precise attitude as well as trajectory adjustments in response to dynamic atmospheric conditions. Lift is generated as a consequence of the pressure differential between the upper and lower surfaces of the wing, a phenomenon governed by Bernoulli's principle and strongly dependent on the angle of attack. This angle directly affects the distribution of airflow and pressure, thereby modulating the magnitude of the lift force. In applied aerodynamics, the resultant aerodynamic force vector (**P**) is defined as the vector sum of the drag force (**Px**) acting parallel to the relative airflow and the lift force (**Pz**) acting perpendicular to it. The orientation and magnitude of **P** critically determine the aircraft's behaviour in flight, influencing its trajectory, stability margins, and control responsiveness. Figure 1 presents a basis model of aerodynamic forces generation [10].

The primary goals of this study were to conduct aerodynamic measurements of an aircraft model equipped with interchangeable vertical stabilisers featuring varying incidence angles, and to determine their corresponding aerodynamic characteristics.

The scope of the research encompassed the following stages:

- Fabrication and refinement of airframe components, ensuring dimensional accuracy and consistency across all model configurations;
- Assembly and preparation of the experimental setup, including calibration of instrumentation and verification of measurement protocols;
- Aerodynamic testing within a wind tunnel environment, aimed at capturing force and moment data under controlled flow conditions;

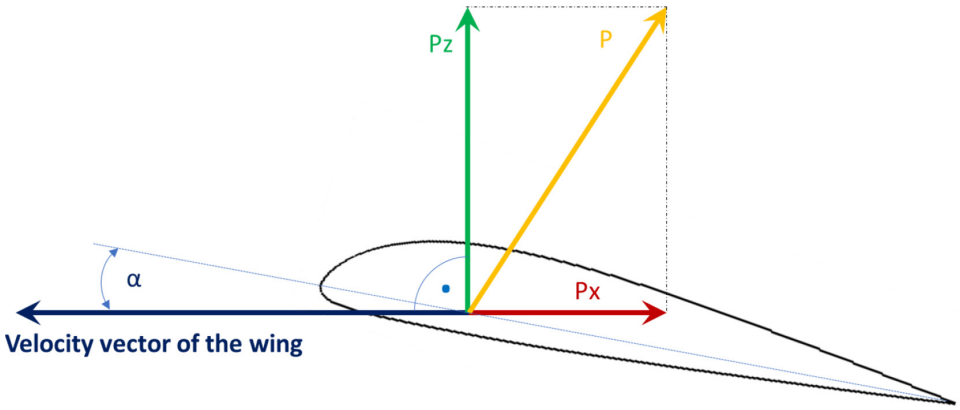

Figure 1. Distribution of forces acting on an airfoil [9]

- Post-processing and analysis of experimental data, followed by graphical visualisation and derivation of aerodynamic performance curves and characteristic plots.

RESEARCH OBJECT AND PREPARATION

The aircraft prototype was designed using advanced computer-aided design (CAD) software and subsequently fabricated through additive manufacturing, specifically employing fused deposition modelling (FDM) with polylactide (PLA) filament (Figure 2). This production method enables high-fidelity replication of intricate geometries while significantly reducing material waste, offering a distinct advantage over conventional subtractive manufacturing processes, such as CNC milling [11].

The structural architecture of the model was intentionally segmented into discrete modules, allowing for streamlined assembly, rapid reconfiguration, and facile replacement of individual components. Of particular experimental relevance is the modular vertical stabiliser system, which permits angular adjustment across seven discrete settings (−15°, −10°, −5°, 0°, +5°, +10°, +15°). This design facilitates systematic investigation into the influence of stabiliser incidence angle on key aerodynamic parameters, including lift, drag, and moment coefficients.

Primary structural configuration of the aircraft model

The structural design of the aircraft model comprises several key components, each fulfilling distinct aerodynamic and mechanical functions:

- Tail section: Serves as a critical aerodynamic appendage, directly interfacing with the central fuselage. Its geometry and placement are essential for maintaining directional stability and controlling yaw during testing.
- Core module: Functions as the central structural element of the model, incorporating a precision-engineered socket designed to accommodate a custom adapter (sleeve). This interface enables secure and accurate mounting onto the wind tunnel balance system, ensuring reliable force and moment measurements under controlled flow conditions (Figure 3)
- Horizontal and vertical stabilisers: These aerodynamic surfaces are integral to the model's stability and control. The horizontal stabiliser contributes to pitch regulation, while the vertical stabiliser governs yaw dynamics. Their precise alignment and modular integration are optimised to maintain consistent airflow and minimise interference effects during experimental trials (Figure 4).

Wind tunnel

Wind tunnel tests enable the analysis of airflow around vehicle models, buildings, or aircraft components under controlled conditions. All measurements and test results were carried out entirely in the wind tunnel located at Lublin University of Technology (Figure 5).

The wind tunnel employed in the study features a modular, closed-circuit design, allowing its configuration to be readily adapted to the characteristics of the tested objects. Airflow is generated by a fan with a diameter of 2400 mm. The side walls of the test chamber are equipped with transparent polymer windows, enabling photographic

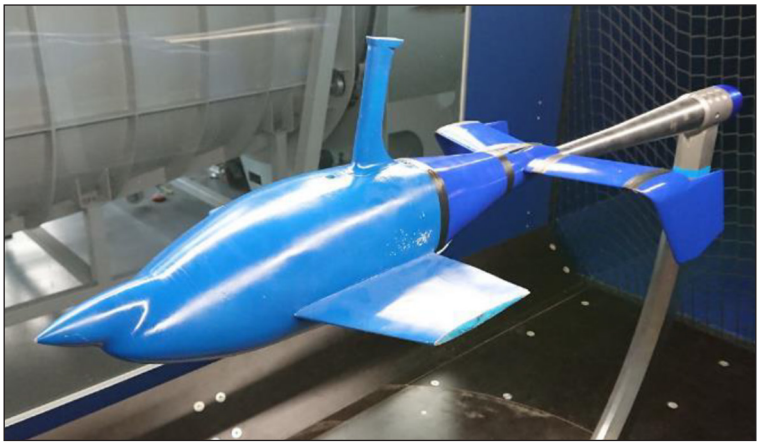

Figure 2. Model view at the measuring station [12]

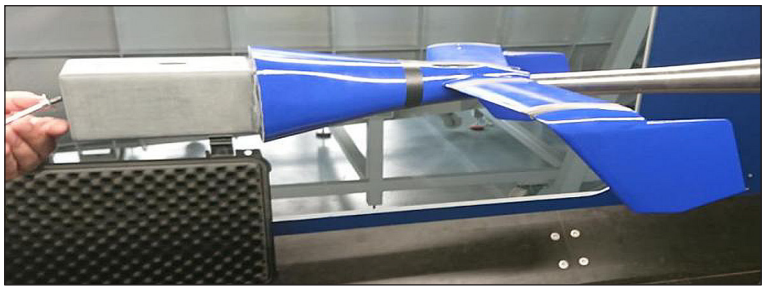

Figure 3. Tail section and core module [12]

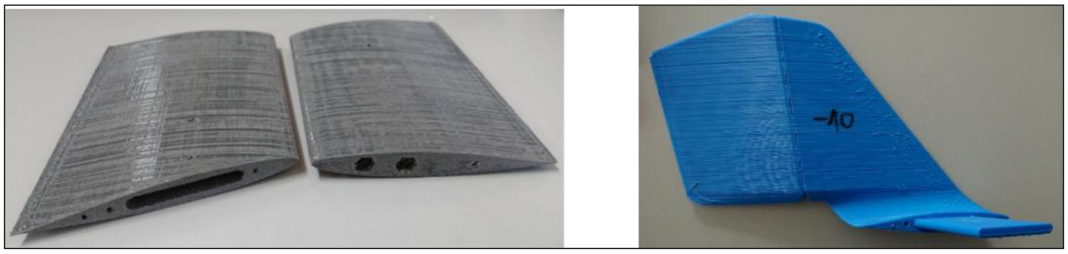

Figure 4. Horizontal and vertical stabilisers [12]

documentation during the measurement process. The facility provides continuous regulation of airflow velocity within the range of 0 to 60 m/s.

Activation of the measurement system and experimental procedure

In the measurement program (Sting), the experimental parameters were defined as follows:

- Airflow velocity was set to 27 m/s to replicate relevant aerodynamic conditions
- Angles of attack α were specified at 0°, +5°, and -5°, while the sideslip angle β was set to +5°, enabling analysis under varied flow orientations,

Before the measurement process begins, a calibration procedure is performed. The test chamber is equipped with an aerodynamic balance fitted with an FMT 618-1b strain-gauge transducer, enabling the measurement of forces and moments in a six-degree-of-freedom coordinate system. The Sting software (Figure 6), which automatically executes the measurement sequence, was used to record the forces and moments.

The airflow velocity around the aircraft model is controlled via the wind-tunnel control panel. Prior to testing, the software requires input of the angle of attack and sideslip angle values, including their increments, as well as the airspeed and air density.

Figure 5. View of the wind tunnel [10]

The measurement range of forces and moments of the strain-gauge sensor is presented in Table 1.

The reference wing area and chord length were scaled according to the geometric scale of the model, based on the actual aircraft dimensions. An additional essential step involved determining the centre of gravity of the model and its offset relative to the aerodynamic balance. This was carried out in SolidWorks by defining reference lines within the model's XYZ coordinate system, using numerical data from the full-scale aircraft. For the tests conducted at an airspeed of 27 m/s, the software generated 126 measurement points. Once the target airflow velocity is reached, the measurement system initiates data acquisition [13]. The collected data are stored in output files and subsequently analysed using tabular and graphical methods, enabling visualisation of the distributions of aerodynamic forces and moments.

Experimental testing of the model

Before commencing the experimental campaign, the free-stream velocity was analysed and selected to ensure that the resulting Reynolds number would be as appropriate as possible for this type of aerodynamic investigation [14, 15].

Using standard laboratory air properties, dynamic viscosity, characteristic dimension

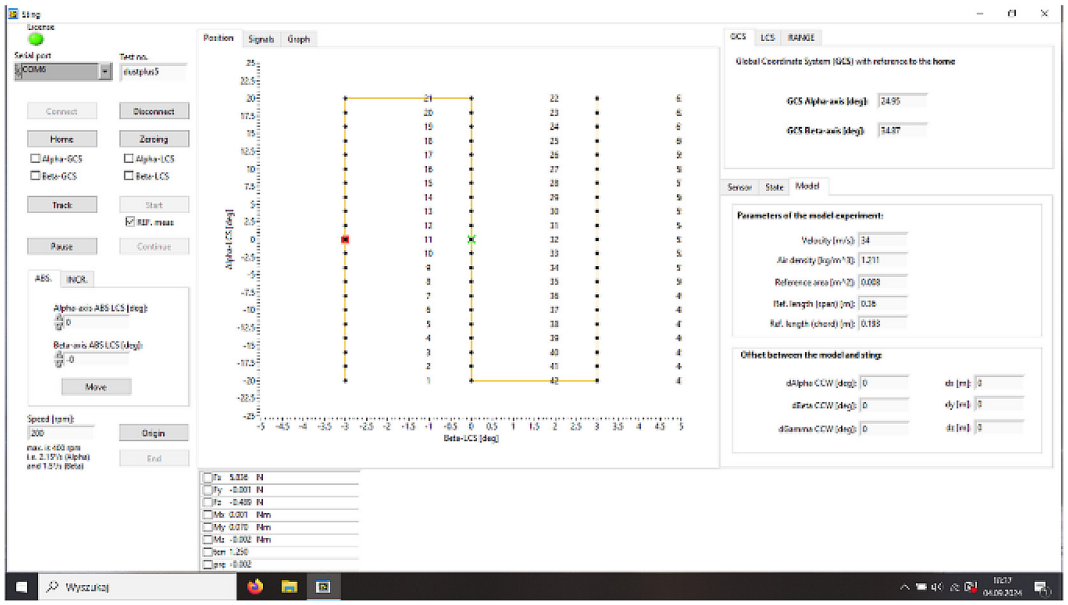

Figure 6. Display of the Sting application interface obtained in the course of measurements [10]

Table 1. Measurement range values of the FMT 618 1b transducer

Measured parameter	Range
F_X	± 170 N
F_Y	± 350 N
F_Z	± 400 N
M_X	± 10 Nm
M_Y	± 19 Nm
M_Z	± 21 Nm

(fuselage length), the Reynolds number corresponding to formula (1):

$$Re = \frac{\rho V L}{\mu} \tag{1}$$

which, when combined with the fuselage length – 637 mm and the air-flow velocity – 27 m/s, yields the final result Re ≈ 1.2 × 10⁶.

Reaching a Reynolds number on the order of one million is of central importance for ensuring that the aerodynamic behaviour observed in the wind tunnel reflects the physical mechanisms present in full-scale flight. [16] At this magnitude, the boundary layer is fully turbulent across the majority of the model's surface, enabling realistic reproduction of flow separation, pressure distribution, and aerodynamic loading. This enhances the reliability of measured lift, drag, and moment coefficients and significantly improves the dynamic similarity between the scaled model and the full-scale aircraft. The selected test velocity of 27 m/s also provides a favourable balance between aerodynamic force magnitude and experimental stability. At this velocity, the aerodynamic loads are sufficiently large to ensure high signal-to-noise ratios in force and moment measurements, while remaining within a range that avoids excessive structural deflection or dynamic instabilities of the model. Lower velocities would place the experiment in a transitional Reynolds-number regime, where the flow is highly sensitive to surface imperfections and exhibits reduced repeatability. Conversely, substantially higher velocities would increase the risk of unwanted aeroelastic effects and introduce unnecessary mechanical loading on the model and mounting system [17].

Operating at 27 m/s therefore ensures:

- A fully turbulent flow regime, enabling realistic modelling of aerodynamic phenomena relevant to full-scale rotorcraft.
- High-quality measurement conditions, with aerodynamic forces large enough for precise quantification.
- Stable and uniform flow in the test section, consistent with the performance characteristics of mid-scale wind-tunnel facilities.
- Reliable extrapolation of aerodynamic coefficients, due to the proximity of the achieved Reynolds number to values used in professional subscale aircraft testing.
- Safe structural loading, preventing excessive deformation or dynamic oscillations that could compromise data integrity.

In conclusion, the calculated Reynolds number of approximately 1.2 × 10⁶ confirms that a free-stream velocity of 27 m/s constitutes an exceptionally well-justified operating point for aerodynamic investigations of the gyrocopter model. This velocity simultaneously satisfies the requirements of dynamic similarity, measurement accuracy, flow stability, and structural safety, making it an optimal choice for controlled experimental research in a closed-section wind tunnel.

The model was prepared in accordance with the procedures outlined in the appendix to this study and subsequently subjected to testing in the configurations specified below:

- Complete autogyro – landing gear retracted
  - Angle of attack: from −25° to +25°
  - Sideslip angle: from −25° to +25°
  - Horizontal stabiliser incidence: from −15° to +15°
  - Rudder deflection: from −20° to +20°
- Autogyro without tail surfaces
  - Without nacelle and landing gear
  - With nacelle
  - With nacelle and landing gear
  - Without nacelle, with landing gear
- Complete autogyro – landing gear extended
  - Angle of attack: from −25° to +25°
  - Sideslip angle: from −25° to +25°

RESULTS AND ANALYSIS

Lift coefficient

The obtained results were processed in tabular form and subsequently used to generate the corresponding plots, which are presented in the following subsections.

The data enabled the development of plots of the lift coefficient c_L as a function of angle of

attack α for different sideslip angles β. Figure 7 presents the graphs for characteristic values of the fuselage sideslip angle β of the autogyro.

Table 2 presents a comparison of the test results for the gyroplane with the landing gear retracted and extended, for various fuselage angles of attack as well as for three different sideslip angles.

From the plots and tabulated data presented in Figure 7, it is evident that the deployed landing gear increases the lift force coefficient for fuselage angles of attack between 0° and 20°, with the most pronounced effect occurring at a sideslip angle of β = 25°. The average increase in the side force coefficient with the landing gear extended is approximately 20%, with the largest numerical increment observed at β = 25° and α = 20° regarding to Equation 2,

$$\Delta_{C_y}\% = \frac{C_{yGR} - C_{yGE}}{C_{yGR}} \tag{2}$$

with corresponding to an increase lift coefficient of about 18% (3).

$$\Delta_{C_L}\% = \frac{C_{LGR} - C_{LGE}}{C_{LGR}} \tag{3}$$

Drag coefficient

Measurement data are presented in the tables that describe the phenomena in detail at each step. For ease of analysis and visualisation, the following subsection provides graphs of the principal characteristics (Figure 8), greatly enhancing the interpretation of the results.

Figure 9 presents the results expressed as the lift coefficient plotted against the drag coefficient, a relationship commonly referred to in the aerospace field as the aerodynamic polar of an airfoil or an aircraft.

The measurement data for the drag coefficient of the autogyro with both the open and enclosed landing gear configurations are presented in Figure 8. For a more detailed assessment, an analysis of the coefficient *k*, which defines the aerodynamic performance, is also provided.

The total drag coefficient is defined by the Equation 4:

$$C_D = C_{D0} + k \cdot C_L^2 \tag{4}$$

where: C_{D0} – parasite drag, $k \cdot C_L^2$ – inducted drag.

Figure 8 provides the data needed to compute the coefficient k, which defines aerodynamic performance as expressed by the Equation 5:

$$k = \frac{1}{\pi e AR} \tag{5}$$

where: AR – wing aspect ratio, e – Oswald efficiency factor.

For simplification purposes and in order to employ numerical data, the coefficient k was

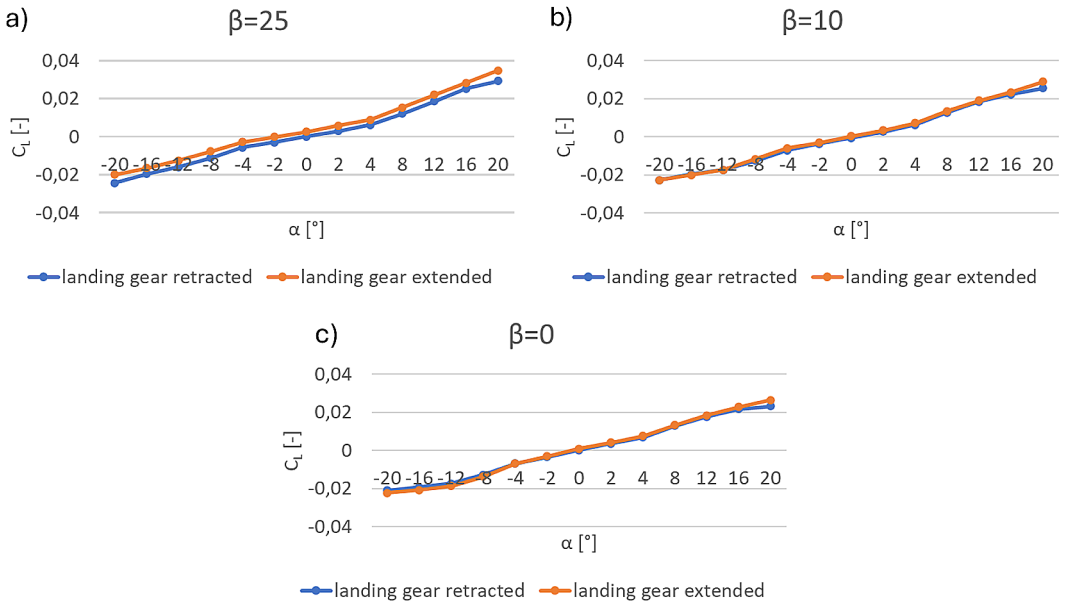

Figure 7. Lift coefficient CL as a function of angle of attack α, a - sideslip angle β=-25°, b – sideslip angle β=-10°, c – sideslip angle β=0°

Table 2. Comparison of lift coefficient values for angles of attack ranging from −25° to +25°, at various sideslip angles β

α [°]	β=0°			β=10°			β=25°		
	C_L LGR	C_L LGE	ΔC_L	C_L LGR	C_L LGE	ΔC_L	C_L LGR	C_L LGE	ΔC_L
-20	-0.0211	-0.0224	-0.0013	-0.0219	-0.0228	-0.0009	-0.0234	-0.0199	0.0035
-16	-0.0197	-0.0207	-0.0010	-0.0201	-0.0201	0.0000	-0.0198	-0.0164	0.0034
-12	-0.0177	-0.0187	-0.0010	-0.0175	-0.0175	0.0001	-0.0158	-0.0125	0.0033
-8	-0.0131	-0.0137	-0.0006	-0.0142	-0.0116	0.0025	-0.0111	-0.0076	0.0035
-4	-0.0071	-0.0069	0.0002	-0.0070	-0.0060	0.0010	-0.0058	-0.0026	0.0032
-2	-0.0037	-0.0030	0.0007	-0.0039	-0.0031	0.0007	-0.0031	0.0000	0.0031
0	0.0000	0.0009	0.0009	-0.0006	0.0003	0.0009	0.0000	0.0027	0.0027
2	0.0032	0.0041	0.0009	0.0026	0.0035	0.0009	0.0033	0.0058	0.0025
4	0.0066	0.0076	0.0010	0.0062	0.0072	0.0010	0.0064	0.0089	0.0025
8	0.0126	0.0133	0.0007	0.0114	0.0136	0.0021	0.0122	0.0155	0.0033
12	0.0176	0.0184	0.0008	0.0184	0.0191	0.0006	0.0191	0.0220	0.0029
16	0.0214	0.0228	0.0014	0.0225	0.0234	0.0009	0.0256	0.0284	0.0027
20	0.0227	0.0265	0.0038	0.0252	0.0289	0.0037	0.0294	0.0348	0.0054

evaluated from the following approximate relation (6):

$$k \approx \frac{C_D - C_{D0}}{(C_L - C_{L0})^2} \tag{6}$$

For comparison, the induced drag factor was estimated using a quadratic regression approach, yielding values of k=13.53 for the landing gear retracted configuration and k=12.09 for the landing gear extended configuration [18] (Table 3). The choice of quadratic regression was motivated by the availability of experimental data and the ability to account for a greater number of real-world effects by fitting the curve directly to the measurement results. The coefficient k calculated directly from Equation 6 does not incorporate actual experimental data and additionally requires the use of a constant Oswald efficiency factor (5).

The measurement data also indicate a slight increase in the drag coefficient when the landing gear is extracted (7),

$$\Delta C_{D0}\% = \frac{C_{D0GE} - C_{D0GR}}{C_{D0GR}} \tag{7}$$

whi,ch results in an increase of approximately 24% for sideslip angle β=0°.

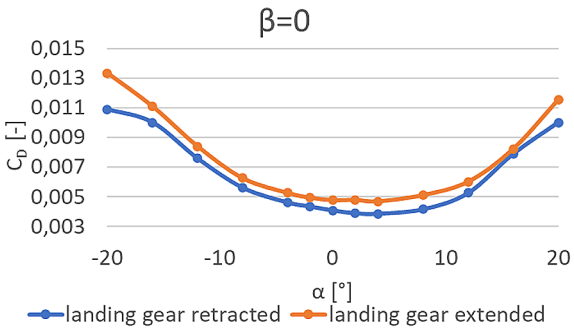

Figure 8. Drag coefficient CD as a function of angle of attack α for sideslip angle β=0°

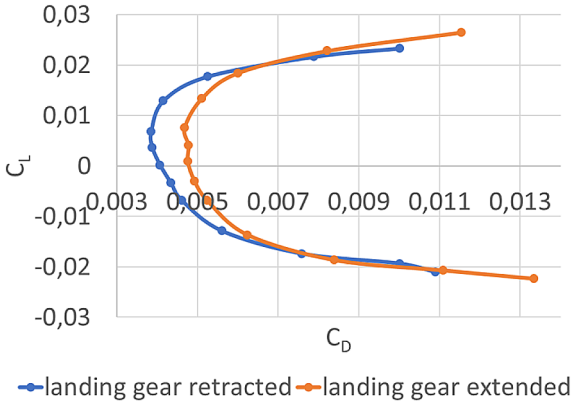

Figure 9. Lift coefficient CL as a function of drag coefficient CD

Pitching moment coefficient

Figure 10 shows the variation of the pitching moment coefficient as a function of angle of attack, which is a key parameter determining the longitudinal stability of an aircraft.

The pitching-moment data shown in Figure 10 make it possible to carry out an analysis of the

Table 3. Lift and drag coefficient values derived from the graph and experimental data, together with the computed coefficient *k*

landing gear retracted		landing gear extended	
C_{D0}	0.00375	C_{D0}	0.00469
C_{L0}	0.00656	C_{L0}	0.00756
k	9.7	k	8.27

autogyro's longitudinal stability. To determine the neutral point, the static margin, and the general longitudinal stability condition, an analytical evaluation was performed.

The pitching-moment coefficient curve can be approximated using an n-th degree polynomial according to Equation 8:

$$c_{my}(\alpha) = a_0 + a_1\alpha + \\ +a_1\alpha^2 + \cdots + a_n\alpha^n \tag{8}$$

In the case of the curve shown in Figure 10 a linear regression is sufficient (9).

$$c_{my}(\alpha) = a\alpha + b \tag{9}$$

Gradient of the pitching moment curve, calculated on the basis of the above plot, is given by:

$$\frac{dcm_y}{d\alpha} = -4.83 \cdot 10^{-4}\ [1/deg]$$

which is equal to:

$$\frac{dcm_y}{d\alpha} = -0.027664\ [1/\text{ rad}]$$

Gradient of the lift coefficient curve, calculated on the basis of the Figure 7a, is given by:

$$\frac{dc_L}{d\alpha} = 1.36 \cdot 10^{-3}\ [1/deg]$$

which is equal to:

$$\frac{dc_L}{d\alpha} = -0.078\ [1/\text{ rad}]$$

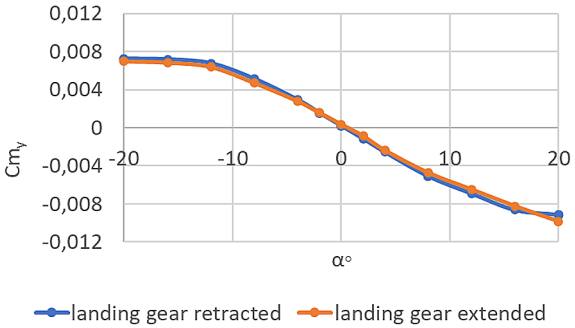

Figure 10. Pitching moment coefficient as a function of angle of attack

Having the above in mind, the position of the neutral point can be determined from Equation 10:

$$\frac{x_{NP}}{c} = \frac{x_{CG}}{c} - \frac{\frac{dcm_y}{d\alpha}}{\frac{dc_L}{d\alpha}} \tag{10}$$

where: x_{CG} – *center of gravity*

By substituting the numerical values, the longitudinal coordinate of the neutral point is obtained, which is relevant for longitudinal stability, equal to $\frac{x_{NP}}{c} = 0.7$, in the context of the center of gravity located $\frac{x_{CG}}{c} = 367$. The static margin is approximately 35.5% of the fuselage length.

Impact of the nacelle

One of the elements of the conducted study was to determine the influence of the nacelle on the generated drag and lift. The autogyro was analysed in the following configurations:

- Autogyro without tail plane, nacelle, and landing gear,
- Autogyro without tail plane, with nacelle.

Figure 11 presents the drag coefficient CD as a function of angle of attack α for the autogyro configuration both with and without the nacelle.

Figure 12 shows the pitching moment coefficient c_{my} as a function of the angle of attack α under the same conditions as above, that is, for the configuration with the nacelle and without the nacelle.

As shown in Figure 11, the fairing causes a significant increase in the drag coefficient, the value of which is as follows (11):

$$\Delta C_{DN0}\% = \frac{C_{DWN} - C_{DN}}{C_{DWN}} \tag{11}$$

where: C_{DN} – *drag coefficient with nacelle*,
C_{DWN} – *drag coefficient without nacelle*.

Figure 11 and Equation 11 indicates that the presence of the nacelle results in an average increase of the drag coefficient exceeding ~50% in case of β=0°.

The slope of the pitching moment curve (Figure 12) as a function of angle of attack is:

$$\frac{dcm_y}{d\alpha} = 6.21 \cdot 10^{-5}\ [1/deg]$$

which is equal to:

$$\frac{dcm_y}{d\alpha} = 0.00356\ ]1//\text{ rad}]$$

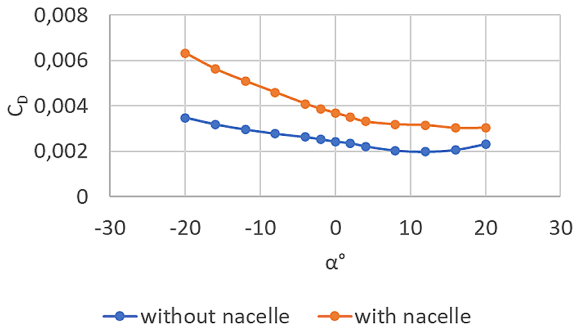

Figure 11. Drag coefficient CD as a function of angle of attack α for the autogyro configuration both with and without the nacelle

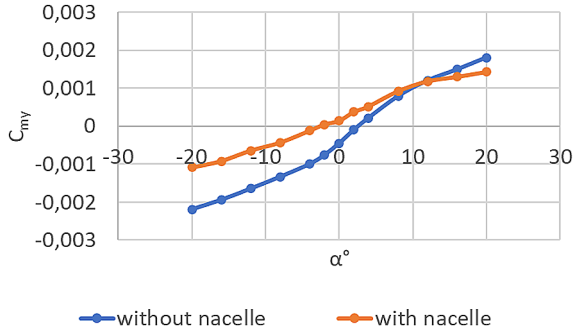

Figure 12. Pitching moment coefficient c_{my} as a function of angle of attack α for the autogyro configuration both with and without the nacelle

The static margin is approximately 21%, as the analogously calculated neutral point is located at $\frac{x_{NP}}{c} = 0.157$, which places it outside the safe stability range.The analysis indicates that the nacelle induces a pronounced pitch-up moment on the autogyro. The absence of a horizontal stabiliser further exacerbates this tendency, resulting in a configuration that exhibits longitudinal static instability [19].

Impact of horizontal and vertical tailplanes

In this subsection, the results of the research and their interpretation were presented for the autogyro equipped with horizontal and vertical tail surfaces. The tests were carried out for various fuselage angles of attack, sideslip angles, and rudder deflections.

Table 4 presents the results of the tests for the autogyro configuration equipped with a horizontal stabiliser for the case study with sideslip angle β = 0.

Figure 13 presents the results of tests for autogiro with horizontal stabiliser. On the basis of Figure 13, the average slope of the lift curve was determined. The horizontal tailplane lift curve slope was calculated according to the formula:

$$a_H = \frac{dC_L}{d\alpha} = 0{,}001552\ [1/deg] = 0.0889\ [1//\text{ rad}]$$

A key parameter for longitudinal stability is the Tail Volume Coefficient, which is determined based on the formula (12):

$$V_{HT} = \frac{S_{HT} \cdot l_{HT}}{S_{rotor} \cdot \bar{c}_{rotor}} \tag{12}$$

where: S_{HT} – horizontal tailplane area, l_{HT} – distance from the aerodynamic center of the tailplane to the aircraft centre of gravity, S_{rotor} – rotor disk area, $\bar{c}_{rotor}$ – mean rotor chord.

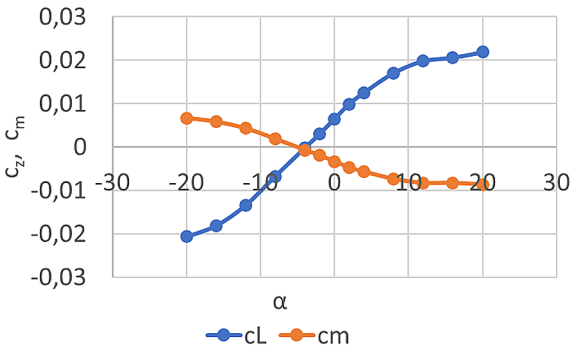

Figure 13. Lift CL and pitching moment coefficient C_m as a function of angle of attack α.

Table 4. Results of the tests for the autogyro configuration equipped with a horizontal stabiliser for the case study with sideslip angle β=0

α	β	c_L	c_m
-20	0	-0.02068	0.006673
-16	0	-0.01815	0.005828
-12	0	-0.01343	0.004289
-8	0	-0.00675	0.001853
-4	0	-0.00022	-0.00071
-2	0	0.003002	-0.00199
0	0	0.006463	-0.00336
2	0	0.009886	-0.00477
4	0	0.012493	-0.00575
8	0	0.017007	-0.00742
12	0	0.019759	-0.00837
16	0	0.02053	-0.00836
20	0	0.021808	-0.00871

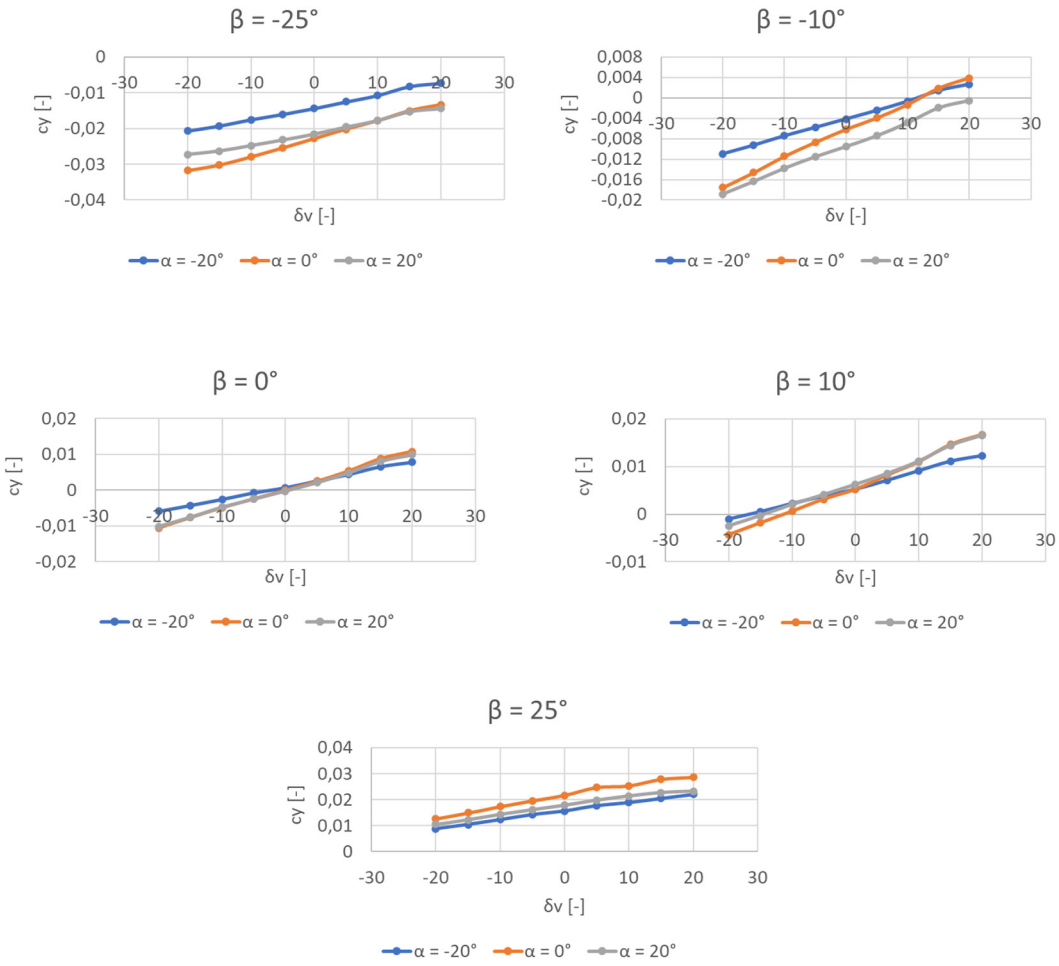

Figure 14. Force coefficient C_y versus vertical stabilizer setting angle δ_v for various fuselage angles of attack α

By substituting the numerical values into the formula, the value of the tail volume coefficient is obtained: $V_{HT} = 0.4685$.

Figure 14 presents the results of the tests for the autogyro configuration equipped with a vertical stabiliser. Considering the result of test presented Figure 14, the mean rate of change of the side force coefficient with respect to the horizontal stabiliser setting angle can be determined using the previously defined analytical expression. Rudder control derivative:

$$a_V = \frac{dC_Y}{d\alpha} = 0.000348\ [1/deg] = 0.0199\ /\ [1/\text{rad}]$$

The analysis indicates that induced drag decreases when the landing gear is deployed, a phenomenon attributed to the significant increase in lift generated by the gear components. Within the examined range of sideslip angles and airspeeds, the extended landing gear enhances the aircraft's overall aerodynamic efficiency. Although the measurement data show a slight increase in parasite drag with the gear extended, the reduction in induced drag partially offsets this penalty, resulting in a net aerodynamic benefit under certain operating conditions. These aerodynamic trends form the basis for evaluating the operational relevance of the landing gear configuration.

CONCLUSIONS

The aerodynamic evaluation conducted in this study demonstrates that the landing gear, nacelle geometry, and tail surfaces exert a significant influence on the performance and stability characteristics of the autogyro. Deployment of the landing gear leads to a marked increase in the drag coefficient; however, at low fuselage angles of attack (−4° to +4°), its effect remains limited. At higher angles of attack, the drag coefficient increases rapidly, while the lift contribution from the gear becomes negligible. These findings indicate that the aerodynamic advantages associated

with extended landing gear are restricted to take-off and landing. For cruise flight, immediate retraction or the application of dedicated fairings is essential to mitigate the associated drag penalty. The rotor-shaft nacelle was identified as a major contributor to fuselage drag, accounting for more than a 50% increase in aerodynamic resistance in its current configuration. The sensitivity of drag to fuselage angle of attack and sideslip underscores the need for geometric refinement of the nacelle and improved aerodynamic integration, particularly through the reduction of sharp edges and discontinuities. The assessment of the autogyro with and without its stabilising surfaces confirms that the horizontal stabiliser provides adequate longitudinal stability. The calculated tail volume coefficient lies within the recommended range, validating the selected stabiliser dimensions and geometry. Similarly, the vertical stabiliser ensures sufficient directional controllability, with only minor rudder deflection required to counteract residual side force.

A fuselage angle of attack of $\beta = 0°$ corresponds to the take-off or landing conditions of a gyroplane. Only under these conditions can the statement regarding improved aerodynamic efficiency be considered valid. As the flight speed increases, the drag produced by the extended landing gear rises rapidly, and the lift coefficient generated by the gear becomes negligible. This shift in aerodynamic behaviour highlights the importance of timely gear retraction.

The analyses above show that deploying the landing gear increases the drag coefficient by approximately 24%, while simultaneously increasing lift by about 6%. This modest lift benefit is relevant only during take-off and flare; for optimal range performance, the gear should be retracted immediately after the rotor becomes fully self-supporting. According to literature [4], wheel fairings could recover roughly 40% of the ΔC_{D0} penalty. Consequently, both operational procedures and design refinements can contribute to improved performance.

Longitudinal static stability requires that $\frac{dcm_y}{d\alpha} < 0$. The slope of the obtained curve is -0.027664/rad, which theoretically satisfies the stability criterion, but in practice this value lies close to neutral stability. This implies the need either to shift the centre of gravity forward or to increase the horizontal stabiliser area. These considerations naturally lead to an assessment of the tailplane geometry.

The horizontal tail volume coefficient for an autogyro should fall within the range of 0.3 to 0.6. On the basis of the conducted analyses and established design guidelines, the size of the horizontal tailplane together with the elevator is sufficient to ensure the required longitudinal stability of the autogyro. Having addressed longitudinal stability, the next step is to evaluate directional control.

The value of the rudder control derivative is approximately 0.02 per radian, which corresponds to a typical effectiveness level reported in the literature for aircraft operating at moderate speeds. The vertical tail surface area is sufficient to provide the required directional controllability. The trim point occurs at approximately −2.76°, indicating that a small rudder deflection is needed to compensate for the residual side force. Overall, the stability and control characteristics fall within acceptable limits for this class of aircraft.

Overall, the results support the validity of the adopted design assumptions while identifying clear opportunities for aerodynamic enhancement.

REFERENCES

1. Houston S., Thomson D., Experimental and theoretical studies of autogyro flight dynamics. ICAS, 2004.
2. Łusiak T., Czyż Z., Magryta P., CFD Numerical Testing for the Effect of Fault. Transactions of the Institute of Aviation, 2013, 232, 3–14.
3. Czyż Z., Kłoda M., Dzaman E., Chabros M., Łusiak T., Comparative analysis of the results of numerical tests of wind turbines with the results of tests in wind tunnels. Technical Transactions, 2013.
4. Łusiak T., Wendeker M., Aerodynamic research of the fusincopter hull, 2/92/NN/2013, Lublin, 2013
5. Łusiak T., Babel R., The initial analysis of the aerodynamic characteristics of a 3D printed model of an aircraft. Journal of KONES Powertrain and Transport,, 2018; 25(4).
6. Stryczniewicz W., Czyż Z., Ruchała P., Łusiak T., Aerodynamic characteristics of windmill hull for different angles of horizontal impact wedging. Transactions of the Institute of Aviation, 2015; 96–107
7. Stalewski W., Computational design and optimisation of innovative, high-efficiency wind turbine. Journal of KONES, 2015; 22(2): 221–232, https://doi.org/10.5604/12314005.1165441
8. Smykała I., Selected aerodynamic and flight

mechanics issues. Warszawa, 2008.

9. Sobieraj W. Aerodynamic, Wojskowa Akademia Techniczna. Warszawa: Wojskowa Akademia Techniczna, 2014.
10. Dudziak J., Gawlik A., Guła P., Tabor M., Ulma D. i Żurawski R., Topology optimization in rotorcraft applications. Netherlands Aerospace Centre, Warszawa, 2022.
11. Łusiak T., Aerodynamic research of an aircraft model. Transportation Research Procedia 2020; 51, 118–133
12. Skoczylas J., Samborski S., Kłonica M., A multilateral study on the FRP composite's matrix strength and damage growth resistance. Composite Structures, 2021; 263, 1–7. https://doi.org/10.1016/j.compstruct.2021.113752
13. Anderson J., Fundamentals of Aerodynamics. McGraw Hill, 2017.
14. Drela M., Flight Vehicle Aerodynamics. The MIT Press, 2014.
15. Pope A., Harper J. J., Low-Speed Wind Tunnel Testing, Wiley, 1966.
16. Kłonica M., Kuczmaszewski J., Samborski S., Effect of a notch on impact resistance of the epidian 57/Z1 epoxy material after "thermal shock". Solid State Phenomena, 2016; 240, 161–167. https://doi.org/10.4028/www.scientific.net/SSP.240.161
17. Anderson J., Fundamentals of Aerodynamics ISE, MCGraw-HIll, 2023.
18. Bernard Etkin L. D. R., Dynamic of flight. Stability and control. Wiley, 1995.
19. Etkin B., Duff Reid L., Dynamic of flight. Stability and control. 1996.